Nonplanar Tests Using the Wind-Tunnel Free-Flight Technique

PETER JAFFE*
Jet Propulsion Laboratory, California Institute of Technology, Pasadena, Calif.

Results from the first biplanar wind-tunnel free-flight test program designed to investigate the difference between planar and nonplanar dynamic stability are presented. The test provides perhaps the best free-flight angular documentation of arbitrary nonplanar motion yet obtained. Two widely different configurations, a blunt 60° half-angle cone and a sharp 10° half-angle cone were tested. Comparisons between the angular motion from raw data and the analytical fits indicate a "phasing" difference. An examination of possible causes discounts experimental errors as an explanation and points strongly toward an inadequacy of the theoretical force model. The dynamic stability results show the same trend for both configurations: a sharp favorable increase in the coefficient as the motion becomes slightly nonplanar, and then a constant decrease as the motion becomes more nonplanar. The data is presented with a newly developed nonplanar correlation parameter which compares the coning to pitch cross-flow velocities. A thorough review of all aspects of the wind-tunnel free-flight data acquisition and data reduction is also presented.

Nomenclature

a to g = tricyclic constants, see Eq. (2)
d = reference length in coefficients, body maximum diameter
p = roll rate, $(I_y/I_x)(\phi_1' + \phi_2')$
$u, v, w,$ = components of velocity; v and w are the transverse components, u is the longitudinal component; $(\tilde{\ })$ refers to nonrolling components; see Fig. 13
x = independent variable, distance between freestream reference and model; see Eq. (2)
A = reference area, $\pi d^2/4$
C_D = drag coefficient
$C_{L\alpha}$ = lift coefficient slope
$C_{m\alpha}$ = static stability coefficient, $\phi_1' \cdot \phi_2'/(\rho A/2m)(md/I_y)$
$C_{mq} + C_{m\dot{\alpha}}$ = dynamic stability coefficient,

$$\left(\frac{I_y}{md^2}\right)\left(\frac{\eta_1 + \eta_2}{\rho A/2m} - C_D + C_{L\alpha}\right)$$

I = moment-of-inertia; subscripts x, y and z refer to moments-of-inertia about the longitudinal and two transverse body axes respectively
K_1, K_2, K_3 = tricyclic vectors: $K_1 = |a + ib|e^{\eta_1 x}, K_2 = |c + id|e^{\eta_2 x}$, and $K_3 = |f + ig|$ [see Eq. (1)]
NPR = Nonplanar ratio, see Eq. (18)
V = magnitude of model velocity; see Fig. 13
α, β = angle of attack and angle of yaw; $\sin\alpha = \tilde{w}/V$, $\sin\beta = \tilde{v}/V$ (see Fig. 13); subscript F refers to fixed-plane axes, see Fig. 8
δ^2 = mean-square resultant angle of attack for flight
$\delta_e{}^2$ = effective squared angle of attack, see Eq. (3)
η_1, η_2 = tricyclic damping constants, see Eq. (2)
θ_H, θ_V = horizontal and vertical model angles, see Fig. 8
ν = rotation of pitch plane, see Fig. 13
ξ = $(\tilde{v} + i\tilde{w})/V = \sin\beta + i\sin\alpha$
ρ = air density
ϕ_1, ϕ_2, ϕ_3 = tricyclic vector angles: $\phi_1 = \phi_{1_0} + \phi_1' x$, $\phi_2 = \phi_{2_0} + \phi_2' x$, $\phi_3 = px$ [see Eq. (1)]
$\hat{\phi}$ = fixed-plane to nonrolling axes transformation angle, see Eq. (8)
ϕ_1', ϕ_2' = tricyclic vector rates; see Eq. (2)
$(\dot{\ })$ = derivative operation with respect to time
$(\ )'$ = derivative operation with respect to x

Presented as Paper 72-983 at the AIAA 2nd Atmospheric Flight Mechanics Conference, Palo Alto, Calif., September 11–13, 1972; submitted September 20, 1972; revision received March 5, 1973. This paper presents the results of one phase of research carried out at the Jet Propulsion Laboratory, California Institute of Technology, under Contract NAS7-100 sponsored by NASA.

Index categories: Uncontrolled Rocket and Missile Dynamics; Entry Vehicle Mission Studies and Flight Mechanics.

* Member of the Technical Staff, Aerophysics Section. Associate Fellow AIAA.

Introduction

PREDICTING the angle-of-attack history of a body exhibiting nonplanar motion from planar data can be erroneous since it presupposes that there are no aerodynamic coupling forces and further requires that the conventional aerodynamic forces which are observable in the planar mode are the same in the nonplanar mode. The investigation of this last requirement was the main purpose of an experimental program conducted in the JPL Supersonic Wind Tunnel using a refined biplanar free-flight system. Specifically, the program was directed toward the question of whether the dynamic stability coefficient is different in the two modes. For this investigation two widely different configurations were chosen: a short, blunt 60° half-angle cone and a sharp 10° half-angle cone. This paper presents the results of this test program.

Test Operation

The basis of the testing technique is to launch models upstream into the oncoming flow with a pneumatic gun.[1] In the case of nonplanar flight, the models are released with an initial angle of attack, yaw angular velocity, and spin rate. The proper combination of these three initial conditions will produce any desired nonplanar motion. This is accomplished by launching the models, which are pneumatically spun about their axis of rotation, at an initial angle of attack and then giving the models a yaw kick at the time they separate from the gun. The motion is recorded with a high-speed 35 mm movie camera operating at about 2000 frames/sec. Two views of the model in flight are obtained by splitting the schlieren strobe light and directing the two beam halves through the test section, approximately 60° apart, by means of a complex mirror system.[2,3] Generally, in excess of 150 frames of data are obtained from a flight. Figure 1 is schematic of the mirror system and Fig. 2 contains a frame of data from the 10° cone test.

Each pair of angles from a frame is measured and mathematically transformed to a vertical and horizontal set. Nominal accuracies for α and β are 0.2° for the slender models and 0.5° for the blunt bodies. In addition to these data, an independent measurement of the model's spin rate is obtained by means of either a fiber optics lens system mounted inside the tunnel, which transmits a picture of the

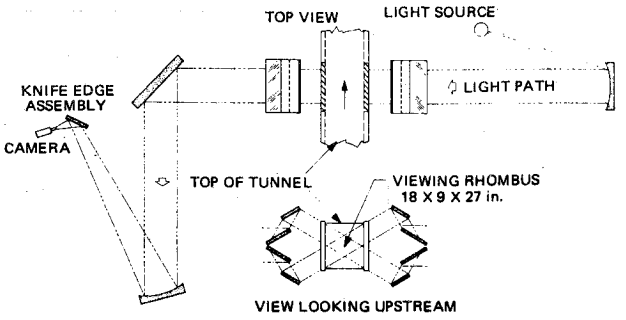

Fig. 1 Biplanar optical system.

model's base to an outside camera, or a stripe painted on the model. The data is processed in a manner similar to the procedure used in a ballistic range, which is to numerically fit the angle data with the tricyclic equation of motion.[4] According to the tricyclic equation α and β are given by the following:

$$\sin\beta + i\sin\alpha = K_1 e^{i\phi_1} + K_2 e^{i\phi_2} + K_3 e^{i\phi_3} \tag{1}$$

and

$$\sin\alpha = e^{\eta_1 x}(a\sin\phi_1' x + b\cos\phi_1' x) + e^{\eta_2 x}(c\sin\phi_2' + d\cos\phi_2' x) + (f\sin px + g\cos px) \tag{2a}$$

$$\sin\beta = e^{\eta_1 x}(a\cos\phi_1' x - b\sin\phi_1' x) + e^{\eta_2 x}(c\cos\phi_2' x - d\sin\phi_2' x) + (f\cos px - g\sin px) \tag{2b}$$

In the fitting process the 10 constants (ϕ_1', ϕ_2', η_1, η_2, and a through g) are determined. These constants define the initial conditions, the roll rate, the trim angle, and the static stability coefficient, the dynamic stability coefficient, and the Magnus moment coefficient. The drag coefficient is obtained independently from the model's translational history. The actual program employed has been improved to account for some of the second order effects. This is discussed in the Test Results section.

The 60° blunt body test was conducted principally at Mach 3.97 with a few shots at Mach 1.65. The 10° cone test was performed at Mach 4.56. The model diameters were 1.0 in. for the 10° cones and 1.5 in. for the 60° blunt cones. The 60° cones were spherically blunted, the nose radius to model base radius was 0.2. The models were designed to optimize the number of pitch cycles and to amplify any change in the angle-of-attack envelope during a flight. This was accomplished by using a dense core and a light plastic exterior shell in the construction; in the case of the blunt cones, gold was used for the cores. Table 1 contains typical model characteristics and test conditions. The 10° cones were launched at spin rates varying from 90 to 135 rps (resonance was about 60 rps). The blunt cone spin rates were from 0 to 35 rps. Here the concept of resonance is not too meaningful because I_x was greater than I_y.

A representative α-β plot from each test is shown in Fig. 3. The stars are the raw data points obtained from the movie frames and the smooth curves are from the fit equations. The standard rms angle-of-attack deviations were typically about 0.4° for the 10° cone flights and 0.8 for the blunt body flights.

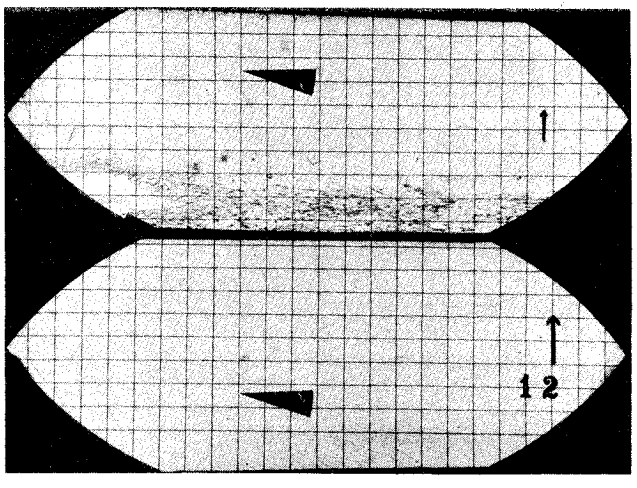

Fig. 2 Typical frame of 10° cone movie data.

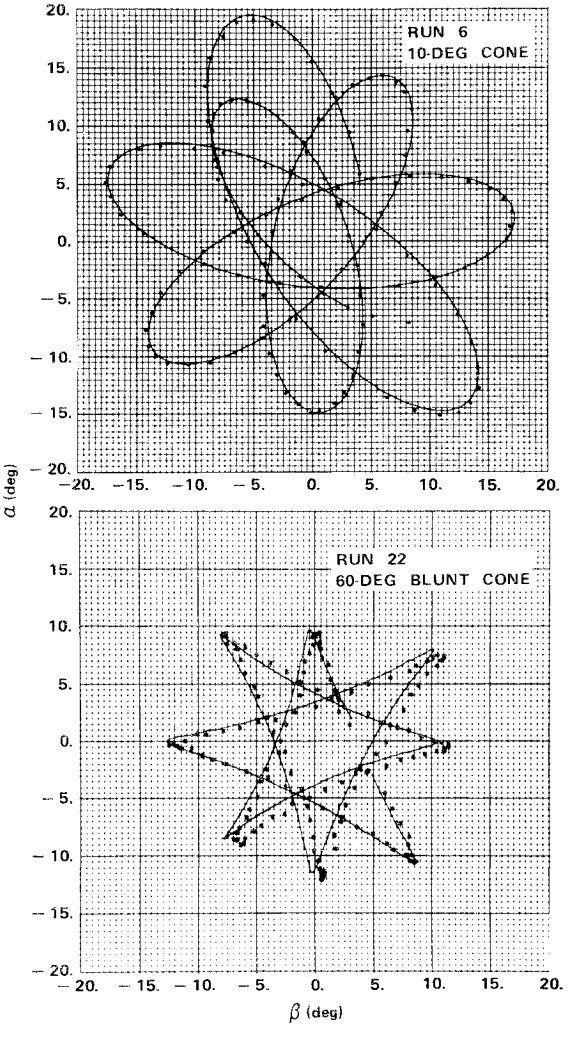

Fig. 3 Typical α-β plots.

Table 1 Typical model characteristics and test conditions

Model	m (slug)	I_y (slug-ft^2)	I_x/I_y	Xcg/d (nose)	Mach	q_∞ (lb/ft^2)	V_∞ (ft/sec)	Re_d
10° cone	0.67×10^{-3}	1.00×10^{-6}	0.194	1.585	4.56	428.	2330.	0.35×10^6
60° blunt cone	0.19×10^{-4}	0.49×10^{-6}	1.45	0.189	3.97	178.	2220.	0.19×10^6
					1.65	218.	1503.	1.13×10^6

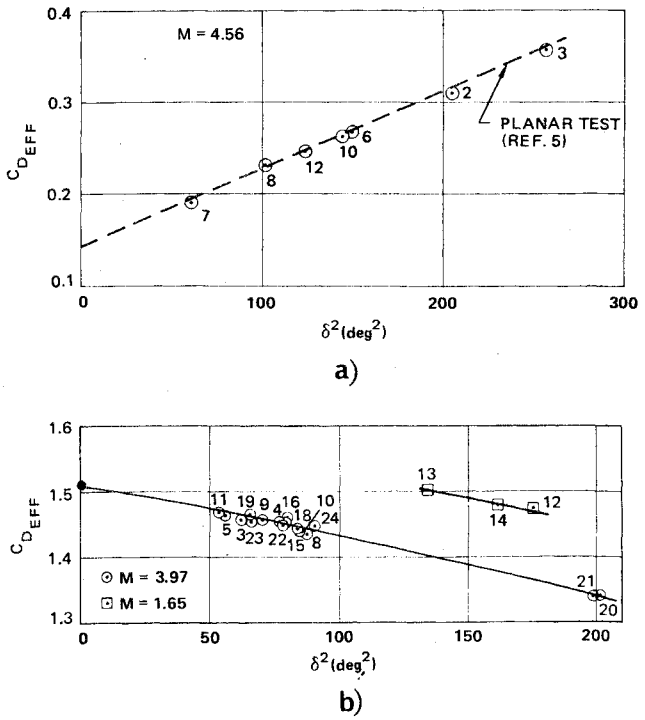

Fig. 4 Drag data: a) 10° cone, b) 60° blunt cone.

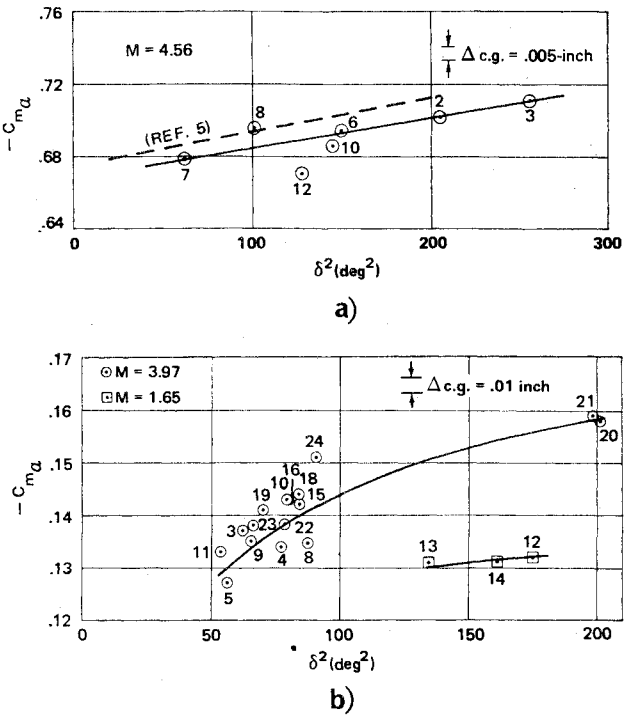

Fig. 5 Static Stability data: a) 10° cone, b) 60° blunt cone.

Drag and Static Stability Test Results

Before proceeding to the dynamic stability data, it is wise to first investigate the drag and static stability results since they provide a gage as to the quality of the data. The drag and static stability coefficients are the results of first-order driving forces and can be obtained much more accurately than the dynamic stability coefficients which are the result of second order forces. If the static data from a flight looks good, confidence in the value of the dynamic stability coefficients is increased.

The drag and stability data are best correlated with the mean-square resultant angle of attack, δ^2. If a body has a local drag coefficient of the common quadratic form $C_D = C_{D_0} + k\delta^2$, then the effective drag coefficient will be of the form $C_{D_{eff}} = C_{D_0} + k\alpha^2$. Figure 4 contains the effective drag data as a function of δ^2 from both tests; the run numbers are next to the data points. The square data points on the blunt body plot are the Mach 1.65 data. The solid circle is from an unpublished previous free-flight test with the same size body at the same conditions. The data from both configurations exhibit almost straight line correlations indicating that the drag coefficients are essentially quadratic functions of the angle of attack. The dashed line on the 10° cone plot is from a previous free-flight test performed in the same facility with the same size and type models.[5] During that test, the motion was planar. The good agreement with the data of this test demonstrate that, as anticipated, drag is not strongly dependent upon the type of motion, but mainly a function of the resultant angle of attack.

Figure 5 contains the static stability data from both tests as a function of δ^2. Both sets of data have been adjusted to the common c.g.'s indicated in Table 1. The 10° cone data increase slightly with δ^2 indicating that the pitching moment is somewhat dependent upon the angle of attack. The data correlate reasonably well with a straight line except for Run 12, which experienced almost circular motion.† This general trend of a linear increasing static stability coefficient is compatible with the previously obtained planar free-flight data, which is summarized by the dashed line.[5] It is believed that the slight difference between the planar and nonplanar data is due to experimental errors. The planar tests were performed several years ago before the model measuring techniques and data reduction procedures were revised. The difference is the magnitude of 0.005 in. in center-of-gravity position.

The blunt body data, which have a fair amount of scatter, exhibit a large increase in the static stability coefficient at large δ^2's, indicating a highly nonlinear pitching moment. The possibility that the scatter was due to an error in the c.g. measurement is negated by the size of the 0.01-in. delta c.g. band shown. The maximum possible c.g. error was 0.005 in. and yet the scatter was far in excess of the 0.01 band. From an investigation of the flights themselves it appears that the individual coefficients are also more accurate than the scatter suggests. This is not surprising since the use of δ^2 as the correlator is not necessarily proper for a nonlinear pitching moment. A vehicle experiencing the same δ^2 during both planar and circular flights will not necessarily have the same effective static stability coefficients. For the case of a cubic pitching moment ($C_m = C\alpha + K\alpha^3$), a good approximate correlator has been developed by Murphy.[6] The correlator δ_e^2, is given by the following expression:

$$\delta_e^2 = (\phi_1'\,\delta_{e_2}^2 - \phi_2'\,\delta_{e_1}^2)/(\phi_1' - \phi_2') \qquad (3)$$

where

$$\delta_{e_{1,2}}^2 = K_{1,2}^2 + 2K_{2,1}^2 + 2K_3^2 + (\text{Trim Terms}) \qquad (4)$$

and the effective C_{m_α} is $C_{m_{\alpha_{eff}}} = C + K\,\delta_e^2$.

Figure 6 presents the Mach 3.97 blunt body static stability data as a function of δ_e^2. The correlation was only somewhat improved. The data seems to best fit the bicubic designation, although insufficient data at the small angles of attack make this only speculation. Another procedure for improving the correlation is to break the flight up into two halves in order to decrease the amplitude effect. This was done for ten of the best runs; the results are shown in Fig. 7 (F denotes the first half and S denotes the second half). There is an

† The tricyclic program cannot accommodate circular motion since for purely circular motion one of the epicyclic vectors is zero. In this case the growth of one of the vectors was inhibited, resulting in a poorer than usual fit.

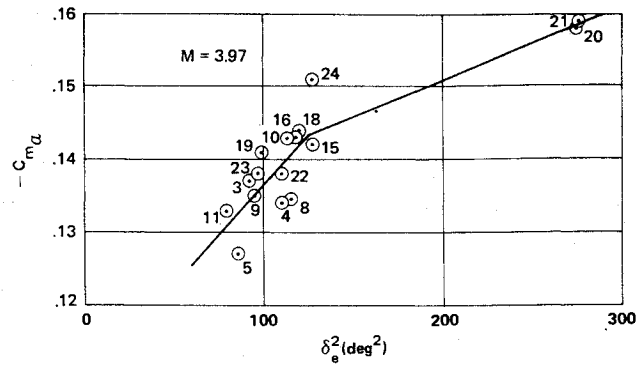

Fig. 6 Static stability data as a function of Murphy's Cubic Correlator.

obvious improvement in the correlation. The real pitching moment probably lies somewhere between the cubic curve of Fig. 7 and the bicubic curve of Fig. 6.

One of the more interesting results from the blunt body test was what appeared to be a phase difference in the generation of the α-β nodes in flight and in theory. A good example of this is Run 22 shown in Fig. 3. The formation of the nodes from the three constant vector rates of the tricyclic fit seem to occur at different times than indicated by the raw data. The basic question that must be asked is whether the difference is real and due to an inadequacy of the theory or is the difference due to flaws in the experimental procedure? In an attempt to determine what caused the "phasing" a complete review of every aspect of both the data acquisition and data reduction was undertaken.

Six possible error areas were postulated and analysed. 1) Errors in determining the pitch and yaw angles with the biplanar system. 2) Errors due to incorrect or improper angles in the data reduction. 3) Errors resulting from the tricyclic assumption of a constant p/V. 4) Nonlinear aerodynamics. 5) Model mass asymmetries. 6) Nonuniform flow.

Biplanar Optical System

To determine the over-all accuracy of the biplanar optical system, the following calibration was performed. Simulated models were put in the tunnel at known angles. The horizontal and vertical components of these angles were then determined with the biplanar optical system and the transformation equations developed in Ref. 2. The results showed deviations occasionally as high as 0.3°. A close examination indicated that a slight optical distortion either in the mirror system, the lens system, or both was present, resulting in a measurable change in a unit length on the movie film. By using the image of the grid, which was composed of accurate 1-in. units, a

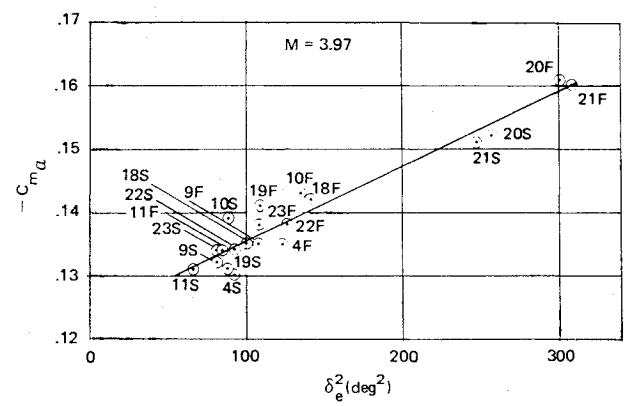

Fig. 7 60° blunt cone static stability results from split flights.

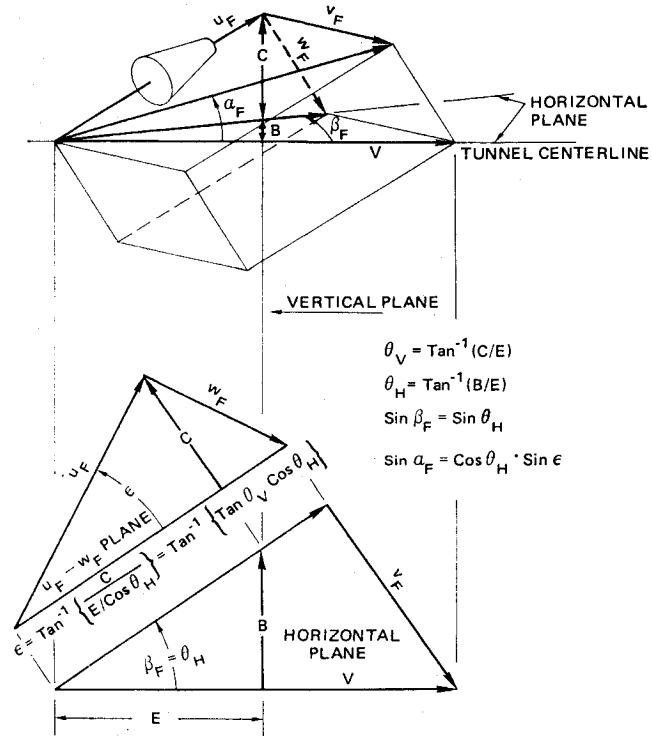

Fig. 8 Fixed-plane axis system.

point-by-point calibration was made. From this calibration a modification of the transformation constants was determined as a function of the model's flight position. The α-β values from typical runs were again determined and inserted into the tricyclic fit program. The results were only slightly improved even though a few of the corrections were as high as 0.3°. The main reason was that the models spent most of their time in the forward half of the window (the model's translational motion is approximately parabolic with time), where the constants were not too different from the original values and the variations small. The excellent correlations of the 10° cone data with the tricyclic fits (Fig. 3) also tend to substantiate that no substantial errors exist in the biplanar system. Nevertheless, additional runs were rereduced with corrected angles but the change in the fits were miniscule.

Angles Used in Data Reduction

There are two problems in using the vertical and horizontal angles in the data reduction. First, they are not quite equivalent to the fixed-plane angles used in the trycyclic equation.[4] Secondly, and more important, the accepted practice of assuming that the fixed-plane angles are almost equivalent to the tricyclic nonrolling angles will produce errors.

Figure 8 shows a model flying in the tunnel and the corresponding axis system. The definitions of α_F and β_F (sub-F refers to fixed-plane) are

$$\sin\alpha_F = w_F/V, \quad \text{and} \quad \sin\beta_F = v_F/V \tag{5}$$

Unfortunately, w_F does not lie in the vertical plane as shown in Fig. 8. In terms of horizontal and vertical angles, the fixed-plane angles are

$$\sin\alpha_F = \cos\theta_H \sin\{\tan^{-1}[\tan\theta_V \cos\theta_H]\} \tag{6}$$

$$\sin\beta_F = \sin\theta_H \tag{7}$$

Therefore, using θ_H and θ_V in lieu of the fixed-plane angles results in an error which is directly related to the model's yaw. For small angles, which is an intrinsic assumption of the

tricyclic equation, this error is small. Nevertheless, it is a simple matter to account for it and this has been done for all the data presented.

The second and more complicated half of the proper angle correction is to convert from fixed-plane to nonrolling axes. This is accomplished in a manner similar to the procedure presented in Ref. 7. From an extension of that work, the following expression for the angle between these two axes systems, $\hat{\phi}$, can be obtained and is presented below

$$\hat{\phi}(x) = \int_0^x \frac{\sin \alpha_F [d(\sin\beta_F)/dx]}{1 - \sin^2\beta_F} dx \tag{8}$$

Unfortunately, in order to evaluate this integral, α and β as functions of x must be known. This is accomplished interatively by first obtaining a tricyclic fit with the fixed-plane angles, using the fit equations to evaluate the integral, and then correcting these angles. Generally, only one interation is required. As an example, Fig. 9 compares the $\hat{\phi}$ history computed with Eq. (8), after one iteration, and the exact $\hat{\phi}$ history obtained from a six degree-of-freedom simulated flight. The comparison is excellent. The process employed was to generate fixed plane angles from a 6-DOF simulation of one of the blunt body flights, Run 21, and use these angles to evaluate $\hat{\phi}$, as if they were real data. A tricycle fit of this simulated flight before the nonrolling correction was made had a rms angle-of-attack deviation of 0.42°. After the correction it was 0.32°. Linear aerodynamics were used to generate the flight. The nonrolling axes transformation only slightly improved the fit even though the accuracy of the transformation had been verified. Obviously, this is only one of the errors that must be taken into account.

Nonconstant p/V and Nonlinear Aerodynamics

Errors resulting from a non-constant p/V and a nonlinear pitching moment both have a direct influence on the epicyclic vector rates (the third vector is the result of an aerodynamic trim which is considered later). Other nonlinearities, such as those related to dynamic stability and Magnus effects have a very small influence since these quantities are intrinsically small for blunt bodies and their nonlinearities have only a second- or third-order influence on the vector rates. The change in p/V for the blunt bodies was due almost completely to a change in V since the influence of roll damping on p was negligible. Data obtained from the fiber optics camera indicated p changed less than 1%, if at all. V, on the other hand, changed about 6% during a typical flight due to deceleration.

From Murphy's work[4] a good approximate solution for the epicyclic frequencies considering only a cubic pitching moment (no amplitude decay, etc.) is

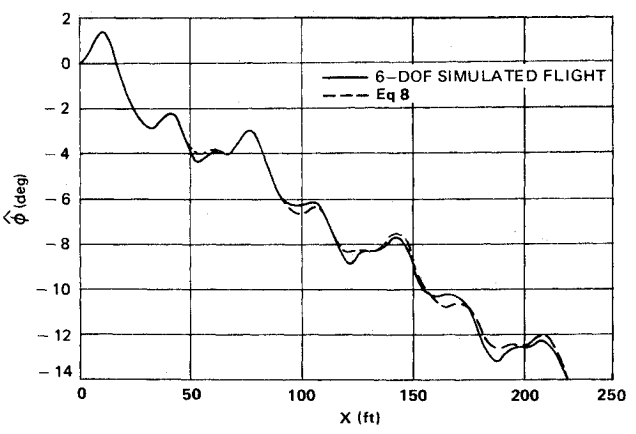

Fig. 9 Comparison of analytical and 6-DOF nonrolling axis transformation.

$$(\phi_{1,2}')^2 - P\phi_{1,2}' + (M_0 + M_2 + \delta_{e_{1,2}}^2) = 0 \tag{9}$$

Where $\delta_{e_1}^2$ and $\delta_{e_2}^2$ (ignoring the trim terms) are

$$\delta_{e_{1,2}}^2 = K_{1,2}^2 + 2K_{2,1}^2 \tag{10}$$

M_0 and M_2 are the linear and cubic pitching moment constants, respectively. The C_{m_α} term has been replaced by $M_0 + M_2\,\delta^2$ in the equation of motion. Considering that only P and δ_{e_1} are variables, and assuming that a change in P is due only to a change in V and that the dynamic stability and drag coefficients are constant, an expression for the ϕ_1'' term can be obtained

$$\frac{d\phi_1'}{dx} = \frac{-2M_2(K_1^2\lambda_1 + 2K_2^2\lambda_2) - \phi_1' P(\rho A C_D/2m)}{(2\phi_1' - P)} \tag{11}$$

Since ϕ_1' and P are changing slowly during the flight, ϕ_1'' is almost constant. Following this premise, an expansion of the vector rates in a Taylor series would give the following

$$\phi_{1,2} = \phi_{1,2_{\text{initial}}} + \phi_{1,2}'x + \tfrac{1}{2}\phi_{1,2}''x^2 \tag{12}$$

Therefore, by adding two more unknowns to the tricyclic fitting process to account for the ϕ'' terms, both the cubic pitching moment and the variation of p/V can be handled. This was done in a 6-DOF simulation of Run 21 using the cubic pitching moment determined from Fig. 7. Figure 10 contains the α-β fits before and after the ϕ'' terms were added. The rms angle-of-atack deviation with the 10-constant program was 0.74°. With the 12-constant program it was substantially reduced to an insignificant 0.05°. The effectiveness of the 12-constant program with a somewhat more nonlinear pitching moment was also considered. Using the bicubic pitching moment determined from the two slopes of Fig. 6 a simulated flight was generated. The rms angle-of-attack deviation of the fit for this case was still an acceptable 0.13°.

The preceding results clearly demonstrate both the importance and effectiveness of using the 12-constant program.

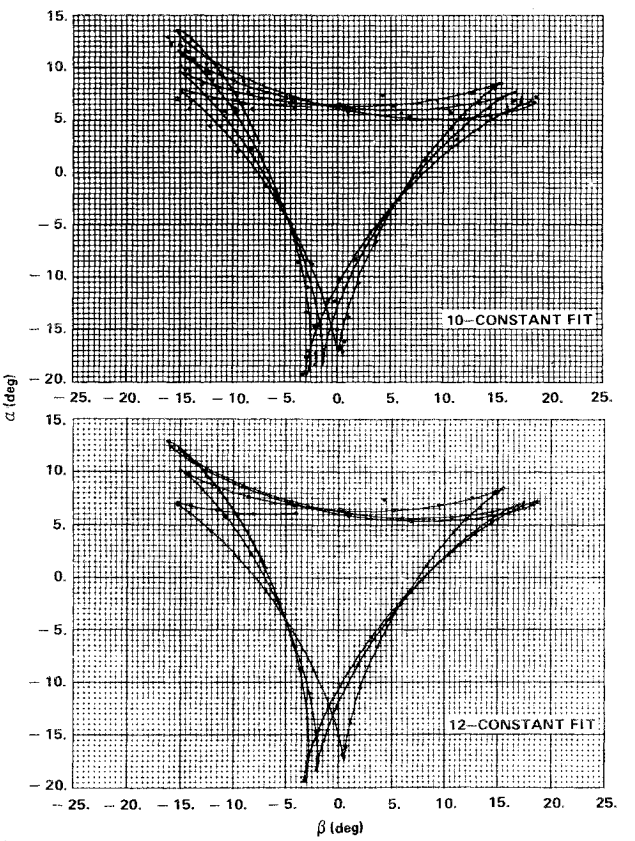

Fig. 10 Tricyclic fits of a 6-DOF simulated flight using 10 and 12 constant programs.

As a consequence, all of the data presented in Figs. 5–7 were processed with the 12-constant program. As it turns out, comparisons of results from the 10-constant and the 12-constant programs using the actual test data show a much smaller improvement than indicated above, generally less than 0.2°. For instance, in the case of the real Run 21 it initially had an rms deviation of 0.92°, with the 10-constant program, and after the corrections it was 0.84°. Although the 12-constant program worked beautifully for simulated data obeying the hypothesized force model, it was insufficient for actual data.

Model Mass Asymmetries

The remaining two errors categories, mass asymmetry and flow nonuniformity, are areas where no data reduction correction can be made. Except for improving the flow and construction of the models, these are errors which must be tolerated.

There are three consequences to not having the model mass on the geometric center-line: first, an aerodynamic trim is generated from the axial force; second, a roll torque is generated from the normal force; and third, the dynamics are affected by unequal transverse moments-of-inertia and cross products-of-inertia. Theoretically, the first is handled by the tricyclic equation if the asymmetry is not too great and the aerodynamics are linear. To investigate the real case where the pitching moment was nonlinear, a trim term was added to the Run 21 Simulation of the previous section. This was done by including an offset c.g. sufficient to produce a trim of 0.67°, per the real Run 21. The corresponding offset was 0.0024 in. The rms angle-of-attack deviation that resulted was 0.11°, or an increase from the nontrim case of 0.06°. Substituting the very nonlinear bicubic pitching moment into the process resulted in an rms angle-of-attack deviation of 0.26°, quite a bit larger than above. Unequal transverse moments-of-inertia were investigated by taking an extreme case where the difference was 2% and including it with the same cubic pitching moment and trim as before. The rms deviation of the fit was 0.29°, a substantial rise of 0.18° over the symmetric moment-of-inertia case. Finally, a case was considered with a cubic pitching moment, trim, transverse moments-of-inertia different by 2%, and a cross products-of-inertia which were larger than probably: $I_{xy} = 0.02\, I_x$ and $I_{yz} = 0.02\, I_z$. The deviation of the fit was a large 0.4°.

In the construction of the models, cast gold cores were used as ballast. Occasionally, they contained air pockets or pits, which destroyed the symmetry. The cores with bad pits were, of course, discarded. It was possible, however, that some of the cores contained air pockets which went undetected to the eye, although a c.g. check on the symmetry of the models was made. Nevertheless, it was possible that one or two had large asymmetries, perhaps even to the level of the last simulated case. On the other hand, most of the flights experienced substantial phasing. Although asymmetries do increase the error, from a statistical point of view considering all the flights made, it seems unlikely that they are the cause of the phasing problem.

Nonuniform Flow

From wind-tunnel calibration data it appears that the maximum possible Mach variation in the total flight rhombus was ±0.015 at Mach 3.97. In the forward half of the flight rhombus (from the middle of the window forward) the variation is half that. In order to gain some insight into what influence this has on the actual motion, the following scheme was devised. Assume that the Mach variation is manifested as a density variation and that the variation is sinusoidal. Further assume, as a worst case, that the variational period is the same as the no spin pitch frequency. For planar motion this would amount to an algebraic increase (or decrease) in the dynamic pressure approximately proportional to the angle of attack. This hypothetical case maximizes the absolute difference between the positive and negative angle-of-attack amplitudes required to balance the pitching moment energy.

A 6-DOF simulated Run 21 was made as described above where the density variation was ±0.02%; this corresponds to the ±0.015 Mach variation. A cubic pitching moment and an offset c.g. per the real Run 21 was assumed. The rms deviation from the fit of this simulation was 0.12° above the uniform flow case. This result is a rather extreme measure of what nonuniform flow can do, as it is unlikely that the density perturbation would vary in the manner hypothesized, but would be more random. More important, the variation in the forward half of the flight rhombus, where the model spends 0.7 of its time, was half as much. Taking everything into consideration, a more realistic error increment due to flow nonuniformity is a small 0.06°.

Table 2 contains a summary of all of the simulated cases run. The table differentiates between results before and after the nonrolling axes correction as well as results from the 10-constant and 12-constant programs.

A final comment: by incorporating the nonrolling correction

Table 2 Rms angle-of-attack deviations in degs of tricyclic fits from 6-DOF simulations of run 21

	Simulation constraint								
Tricyclic program	Linear aerodynamics	Linear aerodynamics p/V held constant	Cubic pitching moment	Bicubic pitching moment	Cubic pitching moment offset c.g. (0.67° trim)	Bicubic pitching moment offset c.g. (0.67° trim)	Cubic pitching moment offset c.g. (0.67° trim) $I_y \neq I_z$	Cubic pitching moment offset c.g. (0.67° trim) $I_y \neq I_z$, I_{xy}, I_{yz}	Cubic pitching moment offset c.g. (0.67° trim) tunnel density varied
10-constant	0.4207	0.2306	0.8045		0.8287				
10-constant with N.R.[a]	0.3222	0.0550	0.7446		0.6266				
12-constant			0.2170	0.2307	0.2297	0.3303	0.3619	0.4578	0.3117
12-constant with N.R.[a]			0.0517	0.1263	0.1094	0.2643	0.2826	0.4081	0.2299

[a] Nonrolling axes transformation.

and constant ϕ'' terms into the basic tricyclic data reduction process, a considerable improvement was obtained. These two improvements very nicely handled both a cubic pitching moment and a changing p/V, as demonstrated by the simulated study, yet they were not very effective in improving the fits with real data. On the other hand, many experimentalists are moving toward even more complicated reduction programs with even higher order nonlinearities in search of better correlations. The force models they are using are about the same as in the tricyclic development, essentially only the degrees of nonlinearity of the coefficients are different. The question that must be raised is: will this approach be successful or is the actual problem not additional nonlinearities, but an inadequacy of the force model?

Dynamic Stability Test Results

The drag and stability results for both configurations indicate a high level of accuracy and consistancy of the test data and provide a measure of credence for the dynamic stability results. Although the "phasing" problem was not reconciled, it seems to have been manifested primarily as a variation in the vector rates and not the vector amplitude decay from which the dynamic stability coefficient is derived. Nevertheless, it should not be ignored altogether since, if this is a flow phenomena, any deviation in the flow model could change the decay mechanism.

The dynamic stability coefficients of both configurations are shown in Figs. 11 and 12 as functions of the mean-square resultant angle of attack. As anticipated, the correlation with δ^2, which is strictly a mean amplitude measurement, is not particularly good. In order to introduce the nonplanar motion into the correlating parameter, Tobak[8] suggested that the coning rate be used as the correlator. After considering this possibility, it was concluded that the coning rate is applicable only when the motion is almost conic; i.e., when the rate is almost constant. An alternate parameter, which embodies the concept of coning and still allows for a

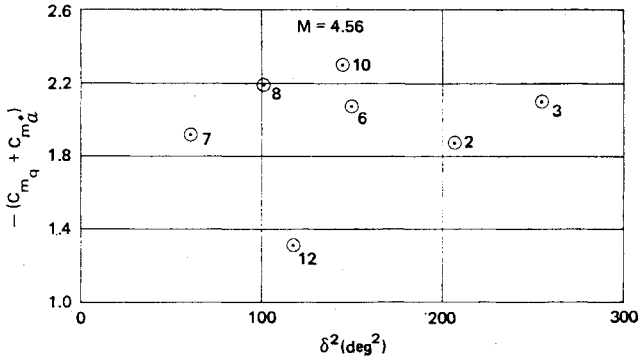

Fig. 11 10° cone dynamic stability data.

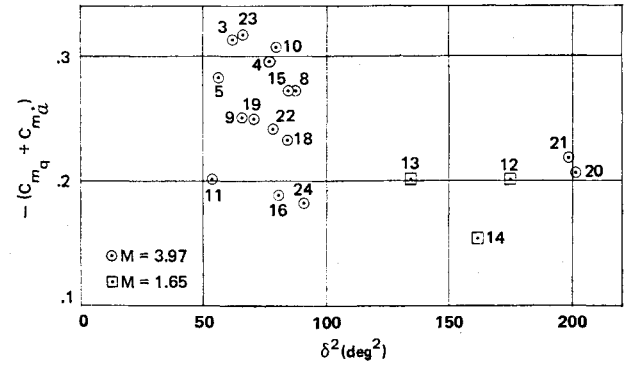

Fig. 12 60° blunt cone dynamic stability data.

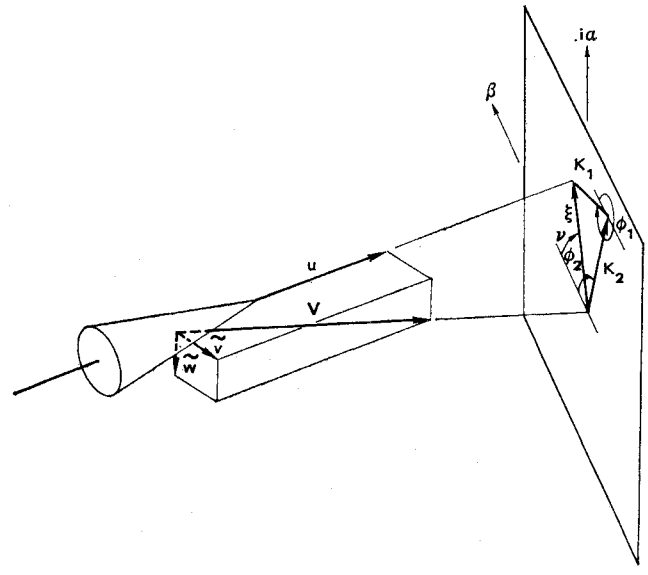

Fig. 13 Epicyclic nomenclature.

variation in the rate, is the ratio of the cross-flow velocity at a point on the body due to coning to the velocity at that point due to pitch.

Figure 13 shows a model in flight and the corresponding α-β plane per the epicyclic equation; for simplicity the trim vector (K_3) has been ignored. The decay of the K_1 and K_2 vectors are assumed to be zero in the following derivation. The pitch plane is defined as the u-V plane and the pitch angle as the absolute value of ξ: (from Ref. 4, p. 143)

$$\xi\bar{\xi} = \delta^2 = K_1^2 + K_2^2 + 2K_1K_2\cos(\phi_1 - \phi_2) \qquad (13)$$

The rotation of the pitch plane about the V axis is denoted ν. From Fig. 14, ν is

$$\nu = \tan^{-1}(K_2\sin\phi_2 + K_1\sin\phi_1/K_2\cos\phi_2 + K_1\cos\phi_1) \qquad (14)$$

The time derivative of ν, or the local coning rate, is

$$\dot\nu = [K_1^2\phi_1' + K_2^2\phi_2' + K_1K_2(\phi_1' + \phi_2')\cos(\phi_1 - \phi_2)/\delta^2]V \qquad (15)$$

Assuming small angles, the velocity of the nose in the direction normal to the pitch plane is

$$\dot\nu\delta l = \frac{\nu'\,\delta l}{V} = \frac{K_1^2\phi_1' + K_2^2\phi_2' + K_1K_2(\phi_1' + \phi_2')\cos(\phi_1 - \phi_2)}{\delta}\,l \qquad (16)$$

where l is the distance from the c.g. to the nose. The pitch velocity at the nose is obtained by taking the time derivative of δ.

$$\dot\delta l = \delta' l/V = [K_1K_2(\phi_1' - \phi_2')\sin(\phi_1 - \phi_2)/\delta]l \qquad (17)$$

The ratio is obtained from the quotient of the mean normal velocity for the flight due to coning to the mean pitch velocity of the flight and is given by the following:

$$\mathrm{NPR} = \int_{x_0}^{x_f} |\nu'\delta|\,dx \Big/ \int_{x_0}^{x_f} |\delta'|\,dx \qquad (18)$$

The subscripts 0 and f refer to the beginning and end of the flight. In practice, this ratio must be obtained by numerically integrating each term. This has been done for all the flights. The dynamic stability coefficients as functions of the Nonplanar Ratio are presented in Figs. 14 and 15. This ratio will be designated NPR.

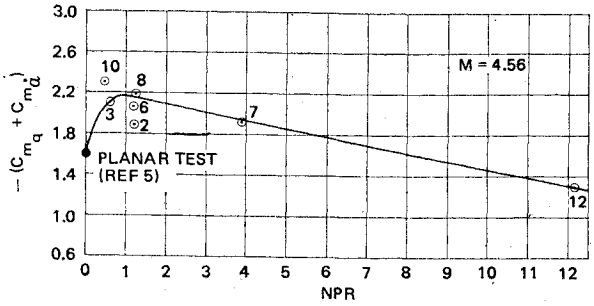

Fig. 14 10° cone dynamic stability data as a function of NPR.

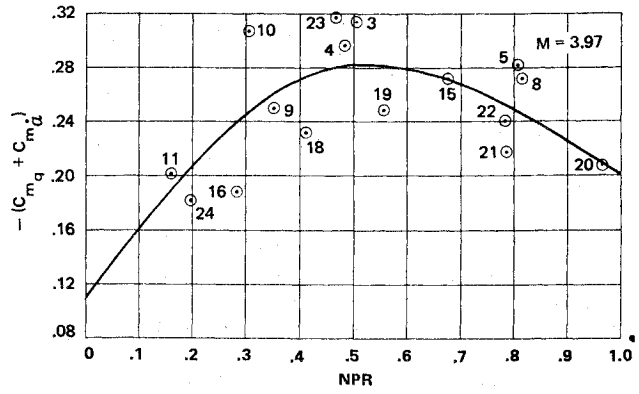

Fig. 15 60° blunt cone dynamic stability data as a function of NPR.

The correlation of the data with NPR shows a marked improvement. Both sets of data demonstrate similar trends; the dynamic stability coefficients increase (negatively) fairly abruptly from their planar values (NPR = O) to peak values and then decrease with increasing NPR. Whether this correlation is fortuitous or the result of some real physical phenomena remains to be seen; the quantity of data is not sufficient to definitely confirm this result. Nevertheless, the fact that both configurations demonstrate the same trend does add credence to it. Considerably more data is needed, particularly at the large values of NPR.

Summary

Using the wind-tunnel free-flight technique and improved instrumentation for the acquisition of nonplanar data, a test program designed to investigate the difference between planar and nonplanar dynamic stability coefficients was performed. This was the first extensive test using the improved nonplanar instrumentation. Two configurations were tested; a blunt 60° half-angle cone and a sharp 10° half-angle cone. The film data from each flight produced between 125 and 250 α-β pairs, providing a thorough and accurate angular motion documentation for each flight; perhaps the most detailed look at arbitrary nonplanar motion yet obtained in a controlled test situation.

Comparisons between the raw α-β plots and the tricyclic fits of the data indicated a "phasing" difference between the two. An investigation to ascertain the nature of this phasing was performed, but nothing conclusive was determined. However, an inadequacy of the force model looks like a possibility. In the process of looking for the cause of the phasing, an extensive review of all aspects of the biplanar free-flight technique was performed resulting in a clean "bill of health" for the technique and the addition of some second-order improvements in the data reduction process.

The dynamic stability data when presented as a function of a nonplanar parameter (NPR), which is the ratio of coning to pitch cross-flow velocities, demonstrates an interesting correlation. At small values of this Nonplanar Ratio (slightly nonplanar motion) the dynamic stability coefficients for both configurations experienced a sharp negative rise (increased stability) and then a gradual decrease (toward less stability) as NPR was increased. This result is only sparsely documented and must be taken as tentative until a more thorough test program is undertaken.

References

[1] Dayman, B., Jr., "Free-Flight Testing in High-Speed Wind Tunnels," AGARDograph 113, May 1966.

[2] Prislin, R. H. and Holway, H. P., "A Wind-Tunnel Free-Flight Testing Technique for Nonplanar Motion of Spinning Models," AIAA Paper 66-774, Los Angeles, Calif., 1966.

[3] Jaffe, P., "Planetary Entry Flight Dynamic Research," *Supporting Research and Advanced Development, Space Programs Summary* 37–62, Vol. III, Jet Propulsion Lab., Pasadena, Calif., April 30, 1970, pp. 218–222.

[4] Murphy, C. H., "Free-Flight Motion of Symmetric Missiles," Rept. 1216, July 1963, Ballistic Research Lab., Aberdeen Proving Ground, Md.

[5] Jaffe, P. and Prislin, R. H., "Effect of Boundary-Layer Transition on Dynamic Stability," TR 32-841, March 1, 1966, Jet Propulsion Lab., Pasadena, Calif.; also *Journal of Spacecraft and Rockets*, Vol. 3, No. 1, Jan. 1966, pp. 46–52.

[6] Murphy, C. H., "Nonlinear Motion of a Missile with Slight Configurational Asymmetries," *Journal of Spacecraft and Rockets*, Vol. 8, No. 3, March 1971, pp. 259–263.

[7] Prislin, R. H. and Jaffe, P., "Evaluation and Extension of the Tricyclic Equation of Motion," AIAA Paper 68–386, San Francisco, Calif., 1968.

[8] Tobak, M. et al., "Aerodynamics of Bodies of Revolution in Coning Motion," *AIAA Journal*, Vol. 7, No. 1, Jan. 1969, pp. 95–99.